Aggregation of Bovine Insulin Probed by DSC/PPC Calorimetry and FTIR Spectroscopy

Wojciech Dzwolak,[‡] Revanur Ravindra,[§] Julia Lendermann,[§] and Roland Winter*[,§]

High-Pressure Research Center, Polish Academy of Sciences, Sokolowska 29/37, 01-142 Warsaw, Poland, and University of Dortmund, Department of Chemistry, Otto-Hahn Strasse 6, D-44227 Dortmund, Germany

Received May 23, 2003; Revised Manuscript Received August 5, 2003

ABSTRACT: Pressure perturbation calorimetry (PPC), differential scanning calorimetry (DSC), and time-resolved Fourier transform infrared spectroscopy (FTIR) have been employed to investigate aggregation of bovine insulin at pH 1.9. The aggregation process exhibits two distinguished phases. In the first phase, an intermediate molten globule-like conformational state is transiently formed, reflected by loose tertiary contacts and a robust H/D-exchange. This is followed by unfolding of the native secondary structure. The unfolding of insulin is fast, endothermic, partly reversible, and accompanied by a volume expansion of approximately 0.2%. The second phase consists of actual aggregation: an exothermic irreversible process revealing typical features of nucleation-controlled kinetics. The volumetric changes associated with the second phase are small. The concentration-dependence of DSC scans does not support a monomer intermediate model. While insulin aggregation under ambient pressure is fast and quantitative, pressure as low as 300 bar is sufficient to prevent the aggregation completely, as high-pressure FTIR spectroscopy revealed. This is explained in terms of the high pressure having an adverse effect on the thermal unfolding of insulin, and therefore preventing occurrence of the aggregation-prone intermediate. A comparison of the aggregation in H_2O and D_2O shows that the isotopic substitution has diverse effects on both the phases of aggregation. In heavy water, a more pronounced volume expansion accompanies the unfolding stage, while only the second phase shifts to higher temperature.

Since formation of the orderly aggregated proteins—amyloids—was found to be associated with several neurodegenerative developments such as Alzheimer's, Huntington's, Creutzfeldt-Jakob's, and Parkinson's diseases (*1*−*3*), and to pose a considerable hassle in biotechnology, the problem of protein aggregation has begun to receive marked attention. The phenomenon, initially thought to concern a handful of proteins, was later observed to be rather common, as amyloid β-fibrils even from otherwise stably folded helical proteins were obtained (*4*, *5*). Mechanisms and thermodynamics lying behind protein aggregation, as well as the relation between aggregation and folding pathways, remain largely unclear. Recently, a hypothesis has been voiced that protein aggregation reflects a generic character of polypeptides as polymers and takes place whenever a polypeptide's main chain interactions are allowed to overrule specific native side-chain contacts in a folded protein (*6*). The presence of such stable tertiary contacts is a distinct feature of folded globular proteins discriminating them from "regular" polymers. Once these contacts are loosened, as it happens in the "molten globule" state, protein molecules become prone to aggregation. This is amply documented by numerous studies on amyloidogenesis under protein-destabilizing conditions such as low pH (insulin (*7*)), point mutations (lysozyme (*8*)), high-pressure (transthyretine (*9*)) or tertiary structure disrupting trifluoroethanol (acylphosphatase (*10*)). As tertiary contacts within folded polypeptide chains and the chains' hydration are two tightly interconnected phenomena, it appears that coupling of the hydration- and structure-sensitive calorimetric and spectroscopic methods can shed new light on the mechanism of protein aggregation.

Fourier transform infrared (FTIR) spectroscopy is a sensitive and commonly used technique of monitoring α-helix-to-β-sheet refolding that accompanies protein aggregation (*11*). It may also be applied to follow changes in protein compactness seen as a progressing H/D-exchange between the protein molecules and heavy water (*12*). Though the conventional FTIR spectroscopy is often used for probing insulin aggregation, the potential of its coupling with H/D-exchange technique has not been explored in this field.

Apart from probing heat-induced transitions in proteins and acquiring thermodynamic data, sensitive differential scanning calorimetry (DSC) methods allow one to inquire into changing hydration of the protein, as enthalpy and partial heat capacity depend on the number of polypeptide chain−solvent contacts and the protein's accessible surface area (ASA) (*13*). This, and the realization of how important an aspect of aggregation is the changing hydration, invite newfound interest in applications of DSC in this field of research (*14*).

A complementary to the DSC set of data on protein−water interactions can be obtained from pressure perturbation calorimetry (PPC), a novel method that allows measurement of heat effects induced by small periodic changes of gas

* Corresponding author. Phone: +49 231 755 3900; fax: +49 231 755 3901; e-mail: winter@pci.chemie.uni-dortmund.de.

[‡] Polish Academy of Sciences.

[§] University of Dortmund.

10.1021/bi034879h CCC: $25.00
Published on Web 09/05/2003

pressure above a protein solution (*15*). The physical principle is the same as in a heat-induced thermal expansion, although the measurable factor is ΔQ, the heat released upon a pressure change of Δp at temperature T. Knowing the thermal expansion coefficient of the solvent, α_s, mass, m, and partial specific volume of the solute, V, through a series of reference measurements, one can calculate the apparent thermal expansion coefficient of the dissolved particle:

$$\alpha = \alpha_s - \frac{\Delta Q}{T\Delta pmV}$$

Furthermore, through stepwise measurements of α in a system undergoing a heat-induced transition and the following integration of the α vs T plot with temperature, the relative volume change accompanying the transition can be calculated:

$$\frac{\Delta V}{V} = \int_{T_1}^{T_2} \alpha \mathrm{d}T$$

PPC yields α vs T plots, which largely reflect the kosmotropic (mostly hydrophobic) or chaotropic (polar and charged) character or amino acid side chain residues interacting with the surrounding solvent (*15*). Dramatic changes in $\alpha-T$ curves observed upon thermal denaturation of proteins arise from different water-structuring properties of amino acids being exposed to the bulk solvent upon unfolding from those interacting with the solvent in the native state. PPC has been successfully used in studies on structural transitions in lipid membranes (*16*), polymers (*17*), and proteins (*15*, *18*). A more comprehensive description of the theory and methodology of PPC was given elsewhere (*15*).

The wealth of biochemical and structural data on insulin and the hormone's ability to aggregate both in vivo and in vitro make it an excellent model for protein aggregation studies. Under physiological conditions, insulin is a hexamer binding two or four zinc ions. With decreasing pH and protein concentration, the association equilibrium is shifted toward smaller oligomers (*19*). At pH 2 and in 20% acetic acid or ethanol, insulin is predominantly monomeric (*20*, *21*). The insulin monomer consists of two chains: a 21-residue-long A chain and a 30-residue-long B chain. The chains are connected by two disulfide bridges, while a third bridge binds Cys residues 6 and 11 of the A chain. The disulfide bridges do not undergo recombination during the aggregation, and the process itself is thought to occur unaccompanied by any covalent modifications of the protein molecule. While only the B chain has been observed to possess an intrinsic ability to aggregate, it does not form amyloid fibrils. Insulin aggregation is fostered under conditions favoring monomers and dimers and partly destabilizing the protein molecule, such as low pH, heat, and contact with hydrophobic media. Several works implicated importance of particular amino acid residues for insulin aggregation (*22*, *23*). For example, the bovine insulin diverging from the human protein at three amino acid positions aggregates much more easily (*23*). While the presence of the B-chain's C-terminal slows down aggregation, the terminal residues at the N-terminal are necessary for the lateral aggregation, i.e., enable protofilaments to form superhelices (*24*). It was shown that insulin amyloid's morphologies and corresponding infrared spectra vary depending on conditions under which the fibrils were grown (*25*). In either case, the fibrils feature typical for amyloids X-ray diffraction patterns, the ability to bind Congo Red and thioflavin T, birefringence, biological dysfunction, and a high degree of stability to temperature, pressure, low pH, and proteases with barely 0.1 M NaOH dissociating insulin fibrils to biologically active oligomers (*26*). The infrared spectra of the amyloid suggest parallel arrangement of the β-strands (*7*), and this remains in accordance with a 3D model proposed for insulin amyloid fibrils (*24*). Some studies have indicated that insulin aggregation can be triggered by nonspecific interactions with hydrophobic environments, such as Teflon surfaces (*27*), air−water (*28*), or water−organic solvent interfaces (*29*). On the other hand, influence of point mutations, concentration, pH, ionic strength, denaturants, organic dyes, etc. on the kinetics of insulin aggregation have been studied as well (*23*, *28*). Hydrostatic pressure of 300−400 bar has been observed to completely prevent aggregation of insulin even under conditions strongly promoting fibrilization (*30*). It is often iterated that insulin aggregation is likely to proceed through a monomer, although the fastest aggregation of insulin is achieved under conditions promoting its dimers (in HCl or H_2SO_4) rather than monomers (in 20% acetic acid) (*19*).

In this work time-resolution, H/D-exchange-perturbation, and pressure-tuning have been coupled with the conventional FTIR spectroscopy to gain a deeper insight into the scenario of biophysical events during insulin aggregation, whose enthalpic and volumetric aspects are simultaneously monitored by the DSC, ITC, and PPC methods.

MATERIALS AND METHODS

Samples. Bovine pancreatic insulin was purchased from Sigma, USA. D_2O and DCl were bought from Aldrich, Germany. For infrared measurements, insulin was typically dissolved at 2% concentration in D_2O. pD was adjusted to 1.9 with diluted DCl. Clear samples were incubated for 1 h at 10 °C prior to recording the first spectra to complete deuterium-substitution of solvent-exposed fast-exchanging amide protons. For calorimetric measurements, insulin was dissolved in either H_2O or D_2O and its pH (pD) was adjusted to 1.9 with diluted HCl or DCl, respectively. A typical sample's concentration was 2%, unless otherwise noted. Throughout all experiments, only fresh samples were used.

Fourier Transform Infrared Spectroscopy (FTIR). For conventional time-resolved FTIR spectra, CaF_2 transmission windows and 0.05-mm Teflon spacers were used. Temperature in the cell was controlled through an external water-circuit and was gradually increased at the rate of 20 °C/h (from 10 to 70 °C) and then kept constant at 70 °C.

For pressure-tuned FTIR, a diamond anvil cell (High-Pressure Diamond Optics Inc., USA) was used. The samples were placed together with α-quartz as internal pressure calibrant into a 0.45-mm diameter hole of a 0.05-mm-thick gasket made of stainless steel (*31*, *32*).

All the FTIR spectra were collected on a Nicolet Magma 550 FT-IR spectrometer equipped with a liquid nitrogen-cooled MTC detector. For each spectrum 256 interferograms of 2 cm^{-1} resolution were co-added. The sample chamber was continuously purged with dry CO_2-free air. From each sample's spectrum a corresponding D_2O spectrum was subtracted. All data processing was performed with OMNIC

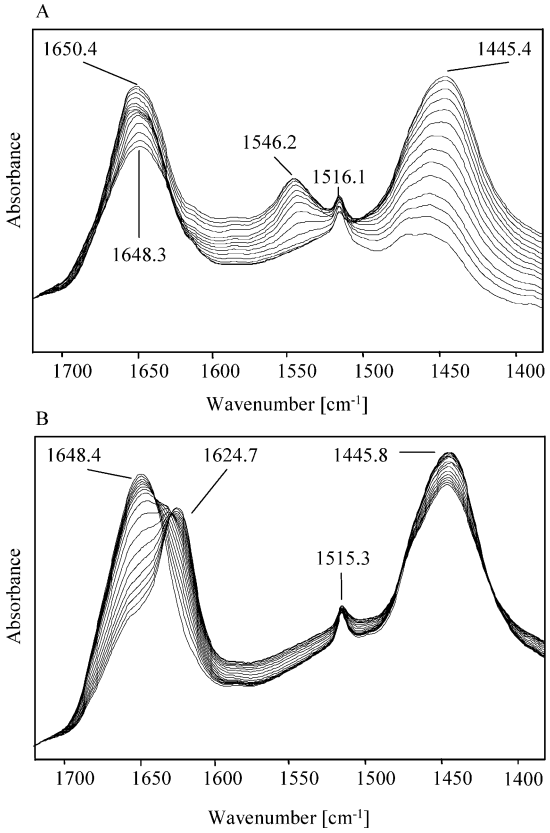

FIGURE 1: FTIR spectra of 2% bovine insulin in D_2O, pD = 1.9 upon gradual heating from 10 to 70 °C at 20 °C/h heating rate (A), and the following time-resolved FTIR spectra of aggregating insulin at 70 °C after complete H/D-exchange (B).

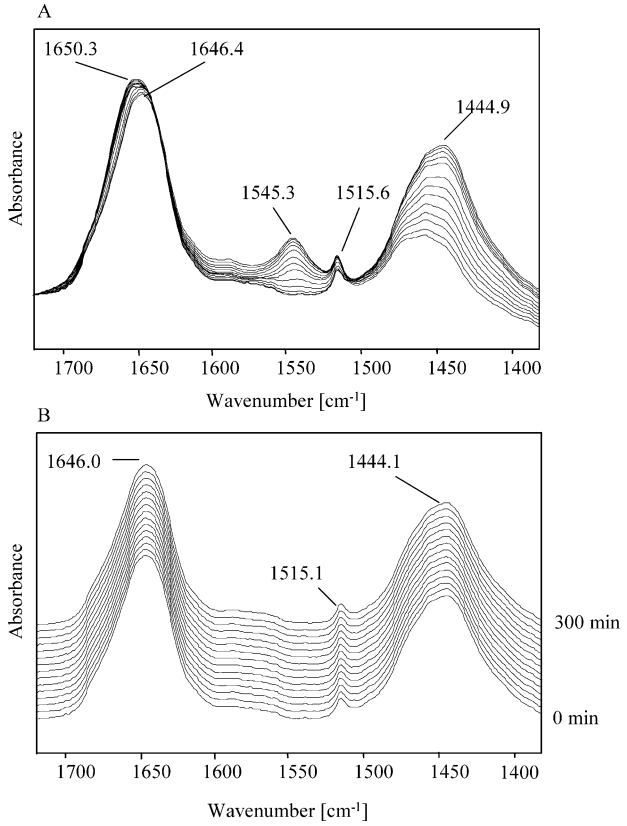

FIGURE 2: FTIR spectra of 2% bovine insulin in D_2O, pD = 1.9 upon gradual heating from 10 to 70 °C at 20 °C/h heating rate under pressure of 300 bar (A), and the following time-resolved FTIR spectra of insulin corresponding to the subsequent 5 h of heating at 70 °C, 300 bar (B).

software (Nicolet, USA) and GRAMS software (Thermo-Nicolet, USA).

Differential Scanning Calorimetry (DSC) and Isothermal Calorimetry (ITC). Differential scanning calorimetry and isothermal scanning calorimetry measurements were carried out on a VP DSC calorimeter from MicroCal (Northampton, MA). The calorimeter's sample cell was filled with ca. 0.5 mL of solution, while the reference cell was filled with a matching buffer. Details of scan rate and temperature range are specified in figure captions.

Pressure Perturbation Calorimetry (PPC). Pressure perturbation calorimetry measurements were carried out on the VP DSC calorimeter equipped with MicroCal's PPC accessory. An extensive description of the technique is placed elsewhere (*15*). Gas (N_2) pressure jump applied to the samples was 5 bar. Under the same experimental conditions, a set of reference sample−buffer, buffer−buffer, buffer−water, and water−water measurements was carried out each time. Specific values of temperature increment per pressure jump circle, scan rate, and temperature range are placed in figure captions and text. The value of partial specific volume of insulin used for volumetric calculations was 0.71 $cm^3\ g^{-1}$.

RESULTS

FTIR. Bovine insulin upon gradual heating from 10 to 70 °C was monitored by FTIR spectroscopy (in Figure 1A). Recorded at a constant 20 °C/h rate spectra encompass the initial 3 h of the experiment. Under these conditions, heat-induced changes of the amide I/I′ band consist mostly in marked broadening of the band, while its intensity maximum shifts from 1650.4 to 1648.3 cm^{-1}. At the same time, a sensitive yardstick of the extend of protein deuteration, the amide II band shifts dramatically from 1546.2 to 1445.4 cm^{-1}. The final spectra recorded above 60 °C are featureless around 1550 cm^{-1}, indicative of the complete H/D-exchange. Since the temperature reached 70 °C it was kept constant for the five following hours and the corresponding time-resolved FTIR spectra are shown in Figure 1B. Upon the prolonged heating of insulin, the amide I′ band starts to undergo pronounced changes in shape shifting its intensity maximum from 1648.4 to 1624.7 cm^{-1}. This reflects appearance of β-strands due to insulin aggregation (*7*). The wavenumber corresponding to the β-sheet aggregate suggests parallel arrangement of the strands. Normalization of integral intensity of the amide I′ band (data not shown) revealed that the transition has only one isosbestic point at 1636.1 cm^{-1}. Thus, FTIR spectroscopy points to no specific intermediate structural states (i.e., having distinct infrared features and distinct secondary folds) that would transiently appear at the isothermic stage of the heating. During both the H/D-exchange and the aggregation, a minor band at 1516 cm^{-1}, assigned to tyrosine (*33*), remains intact.

As hydrostatic pressure is known to dissociate protein assemblies (*34*) and prevent insulin aggregation (*30*), high-pressure FTIR has been applied for monitoring changes that increasing temperature induces in insulin structure under hyperbaric conditions. Figure 2A shows a set of FTIR spectra recorded under the same conditions as in Figure 1A, apart from the pressure being elevated from 1 to 300 bar. As opposed to the atmospheric pressure case, the broadening

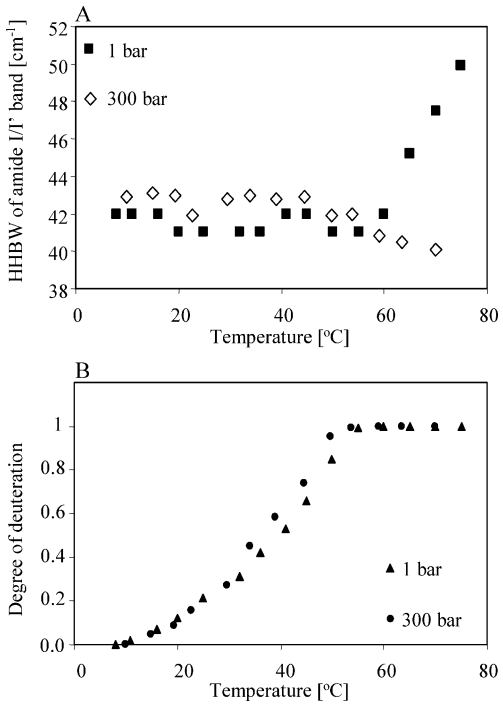

FIGURE 3: The broadening of the amide I/I′ band (A) and the progress of H/D-exchange (B) in bovine insulin (2% solution in D_2O; pD = 1.9) upon gradual heating from 8 to 70 °C (heat rate 20 °C/h). The spectral band's broadening is approximated by the half-height bandwidth, while the H/D-exchange is monitored as a decay of the amide II band at 1 and 300 bar. The upper plateau in figure B corresponds to the completely deuterated protein.

of the amide I/I′ band does not take place, although the band does shift from 1650.3 to 1646.4 cm^{-1}. Otherwise, the course of the H/D-exchange-related spectral changes resembles the case seen in Figure 1A, as the amide II′ band gradually gains intensity at the expense of the amide II band at 1545.3 cm^{-1}. After reaching 70 °C, the temperature has been kept constant for 5 following hours. The corresponding time-resolved infrared spectra are shown in Figure 2B. On the contrary to the ambient-pressure conditions (Figure 1B), no changes in amide I′ band can be detected, implicating intact secondary structure. Figure 3 delineates in a semiquantitative manner the spectral changes observed upon the stepwise heating. The progressing H/D-exchange process has a contribution to the fluctuations of the half-height bandwidth of the amide I/I′ band (Figure 3A). Yet, while the values corresponding to the 300 bar experiment remain approximately constant, under the atmospheric pressure the peak starts to broaden markedly once the temperature reaches 60 °C. At 75 °C, the band maximum has shifted toward lower wavenumbers and the bandwidth is roughly 25% larger than for the native insulin at room temperature, which indicates that the protein conformation is dominated by disordered structures. A small, yet visible H/D-exchange-enhancing pressure effect can be concluded from Figure 3B, which depicts the gradual decay of the amide II band under 1 and 300 bar. In either case, the deuteration is complete at 55 °C.

DSC, ITC, and PPC. The aggregation of bovine insulin was then followed by differential scanning calorimetry (DSC) under identical sample conditions and similar heating regime as in the case of the infrared measurements. Heavy water was replaced with H_2O for most of the measurements and the relevance of this substitution has been examined and

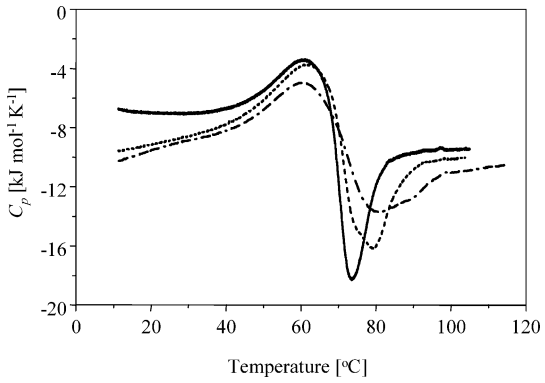

FIGURE 4: DSC scans showing apparent molar heat capacity curves of aggregating bovine insulin (2% solution in H_2O; pH = 1.9) at different scan rates: 10 °C/h (solid line); 20 °C/h (dotted line); 30 °C/h (dash dot line).

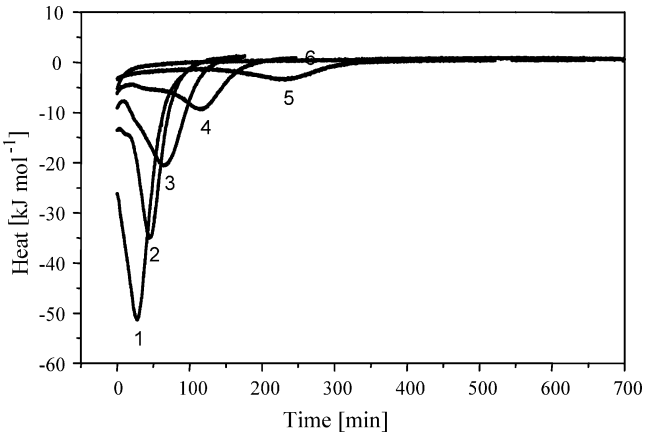

FIGURE 5: Isothermal calorimetry curves corresponding to the heat released by aggregating bovine insulin (2% solution in H_2O; pH = 1.9) at different temperatures: **1**: 80 °C; **2**: 75 °C; **3**: 70 °C; **4**: 65 °C; **5**: 60 °C; **6**: 55 °C.

analyzed later (Figures 9 and 10). All samples were loaded at 7 °C and equilibrated at that temperature for about 15 min before the experiment was started. Figure 4 displays DSC scans of 2% bovine insulin taken at three different scan rates: 10, 20, and 30 °C/h. The 20 °C/h scan rate corresponds to the conditions applied in the infrared study (Figures 1A, 2A, and 3). All three DSC scans feature a positive peak arising from an endothermic transition at 60 °C, which precedes another, exothermic transition. The changing scan rate has little effect on the shape and position of the endothermic peak, but it does influence both these traits of the exothermic peak. Namely, the higher the scan rate is, the broader and more shifted to higher temperature the peak becomes. At every scan rate applied, an extrapolation of the baselines of the DSC curves gave a value of the apparent heat capacity of the native protein of approximately 2 kJ mol^{-1} K^{-1} higher than that of the completely aggregated protein.

To determine the exothermic effects of insulin aggregation, also isothermal calorimetric (ITC) scans were carried out. A sample was initially heated to a desired temperature range through a fast DSC scan. Once the temperature was reached, it was kept constant and the experiment continued in the ITC mode (Figure 5). At 55 °C aggregation is apparently too slow to be detected within the experimental time frame; however, at 60 °C the effect is already measurable and the aggregation accelerates rapidly with increasing temperature

Table 1. Heat Effects of Aggregating Bovine Insulin (2% solution in H_2O; pH = 1.9) Measured during the ITC Scans at Different Temperatures

temp [°C]	ΔH [kJ mol^{-1}]	time passed until peak's minimum [min]
55 ± 1	no transition	
60 ± 1	−16 ± 0.15	232
65 ± 1	−30 ± 0.15	122
70 ± 1	−53 ± 0.15	69
75 ± 1	−57 ± 0.15	48
80 ± 1	estimation unfeasible	28

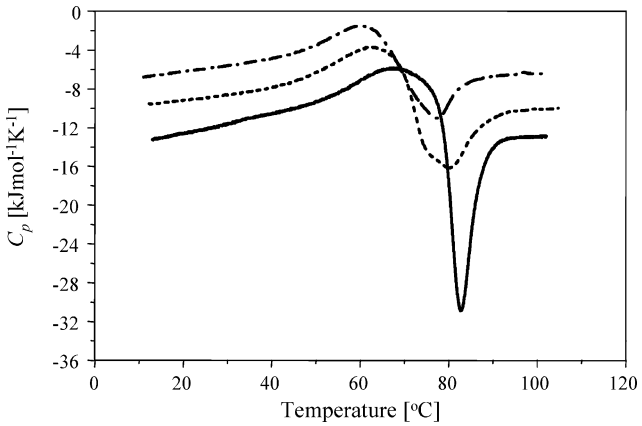

FIGURE 6: DSC scans showing the apparent molar heat capacity curves of aggregating bovine insulin (20 °C/h scan rate; solution in H_2O; pH = 1.9) at different concentrations of insulin: 1% (solid line); 2% (dotted line); 3% (dash dot line).

further on. The data in Table 1 show that increasing aggregation rate was concomitant with an increasingly exothermic character of this process. At 80 °C and above, estimation of heat effects was unfeasible, as the process apparently begins even before the temperature of the ITC scan is reached.

The concentration effect on DSC curves is shown in Figure 6. Increasing concentration influences both the endothermic and the exothermic transitions, as the corresponding DSC peaks simultaneously shift to a lower temperature range when concentration increases. The previously remarked decrease of heat capacity upon aggregation (Figure 4) clearly holds true for the different protein concentrations. While there are no doubts as to whether the actual aggregation stage (the exothermic process) is irreversible, this is uncertain for the preceding endothermic process. To verify it, a series of DSC scans has been performed. Each scan stopped short of entering the temperature range at which aggregation becomes fast. The results are presented in Figure 7. Each time temperature reached 65 °C, the sample was subsequently cooled to 10 °C. In this manner, four following DSC scans were recorded. Though the second scan still shows the endothermic process taking place, its intensity is reduced by roughly 30−40%. This decrease becomes only exacerbated in the third and fourth DSC scans. The latter scan corresponds to that of a completely aggregated protein, as neither significant endothermic nor exothermic peaks appear.

Pressure perturbation calorimetry was employed to investigate changing thermal expansion and volumetric effects in the aggregating insulin. The sample conditions and the heating regime were either the same or made comparable to those in the DSC and FTIR measurements. Figure 8 depicts

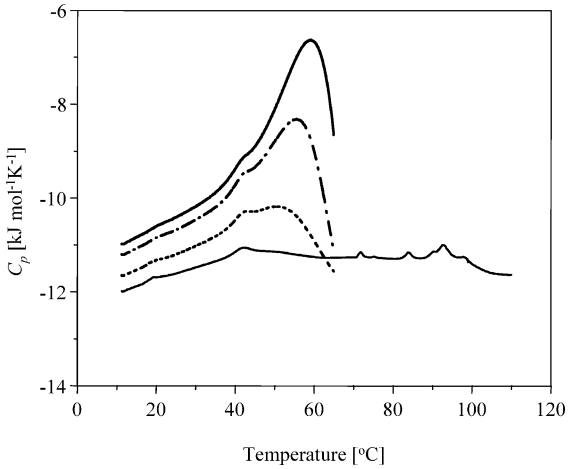

FIGURE 7: Multiple DSC scans stop short before the aggregation phase of bovine insulin (2% solution in H_2O; pH = 1.9; 20 °C/h scan rate). Scan order: first (solid line); second (dash dot line); third (dotted line); fourth, aggregated sample (flat solid line).

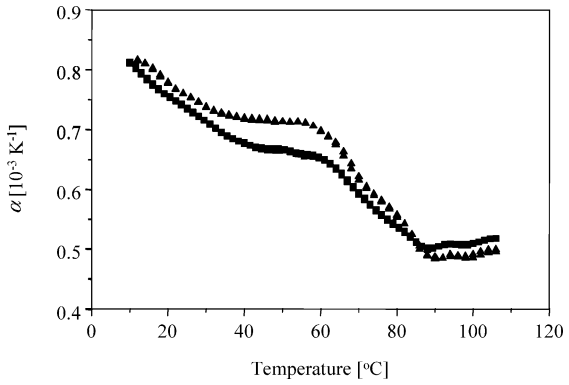

FIGURE 8: PPC curves of bovine insulin (2% solution in H_2O; pH = 1.9) upon heat-induced aggregation. Averaged scan rates are 30 °C/h (triangles); 20 °C/h (squares).

changes of the apparent thermal expansion coefficient of insulin undergoing aggregation. The α values were calculated in a manner described in the introduction. The two plots correspond to two different temperature increments per pressure cycle yielding two effective temperature scan rates of 20 and 30 °C/h. The plots share similar negative temperature-dependences of the α coefficient, which is high at low temperature but diminishes in the higher temperature range. The broad "peak" around 60 °C reflects a volumetric expansion of the insulin sample. Indeed, after a numeric integration of the $\alpha(T)$ curves, the relative volume changes could be calculated. For the consecutive 5, 10, 15 (plots not shown), 20, and 30 °C/h scan rates the relative volume changes were 0.26% (± 0.02), 0.24% (± 0.02), 0.20% (± 0.015), 0.13% (± 0.01), and 0.1% (± 0.01), respectively. The PPC scans show that the volumetric effects of the actual aggregation phase are immeasurably (by the means of PPC) small, as at temperatures corresponding to the exothermic peak in the DSC scans, the α-vs-T plot is essentially flat.

DSC curves of insulin dissolved in H_2O and D_2O are juxtaposed in Figure 9. Heavy water is seen as having a stabilizing effect on insulin aggregation, yet this clearly consists of shifting (by 7 °C) the exothermic, not the endothermic, peak. Another remarkable difference observed upon solvent substitution concerns ΔC_p before the endothermic transition and after the exothermic transition which

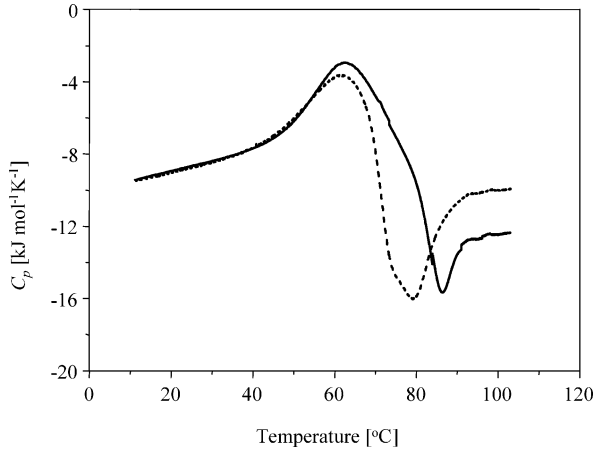

FIGURE 9: Comparative DSC scans of aggregating bovine insulin (2% solution; pH/pD = 1.9; 20 °C/h scan rate) in H_2O (dotted line) and D_2O (solid line).

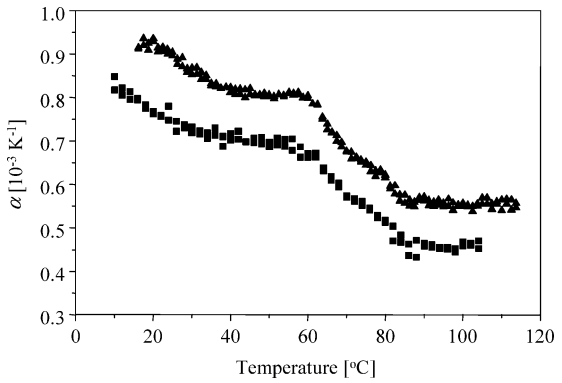

FIGURE 10: PPC curves of bovine insulin (2% solution; pH/pD = 1.9; 20 °C/h average scan rate) upon heat-induced aggregation in H_2O (squares) and D_2O (triangles).

is drastically more negative in heavy water (approximately -4 ± 0.15 kJ mol^{-1} K^{-1}) than in H_2O (less than -2 kJ mol^{-1} K^{-1}).

The effect of H/D isotopic substitution on insulin aggregation has been also investigated through PPC (Figure 10). Though the α-vs-*T* curves of insulin in H_2O and D_2O retain a similar shape, the α values measured for insulin dissolved in D_2O are invariably larger by approximately 1×10^{-4} K^{-1}. The isotopic substitution does not shift the temperature, at which volume expansion is largest (around 58 °C), but it does significantly affect relative volume changes. Namely, at 20 °C/h scan rate, ΔV is 0.13% ($\pm$ 0.01) in H_2O, and 0.35% ($\pm$ 0.025) in D_2O.

DISCUSSION

FTIR Probe of Compactness and Structure of Insulin upon Aggregation. The FTIR data presented in this work portray insulin aggregation as a two-phase process, in which loosening of the native tertiary contacts and the subsequent unfolding precede the actual aggregation. An infrared probe of compactness of protein molecules is only feasible when the protein possesses protected amide protons, which is clearly the case of bovine insulin at pD = 1.9, as the protein is not fully deuterated upon dissolving in D_2O and low-temperature incubation. However, in an NMR study on a close analogue of insulin, DPI (des-pentapeptide insulin) peptide dissolved in D_2O at pD = 1.9, no protected protons were observed (*35*). Compared to native insulin, the DPI peptide lacks the five terminal residues of the B chain, which link two B chains through an intramolecular antiparallel β-sheet in a dimer. Therefore, the absence of protected protons in DPI could be, in part, attributed to its monomeric character. At pD = 1.9, bovine insulin is predominantly a dimer (*19*). Dissociation of dimers does not seem likely to account for the D_2O route into protein's interior and the following H/D-exchange. That is because the dissociation would result in unfolding of the B26−B30 antiparallel β-sheet (10% of all residues) into random coil, which is expected to affect the infrared spectrum (*20*). However, as Figure 3 clearly shows, the H/D-exchange is complete either before the thermal unfolding starts (at atmospheric pressure) or in the absence of changes in the secondary structure (at 300 bar). Therefore, a dimer of insulin that is permissive to solvent-penetration and has nativelike secondary folds seems to occur under the experimental conditions. At the further increasing temperature insulin unfolds into a disordered structure. Because of the common coincidence of the IR wavenumbers corresponding to α-helical structures and random coil (*36*), focusing on the bandwidth rather than on the peak's position becomes a more reliable diagnostic tool of unfolding. Figures 1A and 3 point to the unfolding of already fully solvent exchanged, deuterated insulin to precede the aggregation and refolding into non-native β-sheet. As mentioned before, the normalization of integral intensity of the amide I′ band upon the latter process (Figure 1B) revealed only one isosbestic point at 1636.1 cm^{-1}. Thus, the refolding of the random coil into the β-sheet appears to proceed with no evidence of any distinguished (in terms of the secondary fold) intermediate states.

MG-Like Aggregation Intermediate. Due to the strict unification of sample conditions and heating regime in FTIR, DSC, and PPC experiments, a relative chronology of following phases of aggregation can be analyzed by juxtaposition and comparison of the FTIR, DSC, and PPC data. Insulin is completely deuterated at 50 °C at a 20 °C/h heating rate and starts to unfold at ∼60 °C (Figure 3). The position of the endothermic transition seen in DSC (Figure 4) and the maximum of volumetric expansion observed in PPC plots (Figure 8) are also around 60 °C. These facts can be interpreted as three different aspects of a single transition of insulin molten globule (MG)-like molecule into aggregation-competent unstructured "intermediates". The lack of ordered secondary structure results in an extensive exposition of peptide side-chains to the bulk solvent. This explains the increased heat capacity (DSC), and volume expansion (PPC), as nonpolar amino acid side chains enhance a space-consuming highly structured water network at the peptide's surface (*18*). It should be noted that aggregation of polypeptides and proteins may have either endothermic (e.g., polylysine (*37*)) or exothermic (Co^{2+}/Co^{2+}-phosphotriesterase (*38*)) character, or, as for insulin, an exothermic aggregation may follow after an endothermic intermediate transition (protein C9 (*13*)). Though we are not aware of any studies that explicitly produced evidence of the exothermic character of insulin aggregation, this could have been inferred from the early works by Waught, who observed that preparation of insulin amyloid requires only initial heating, and will continue at room temperature (*26*). It seems crucial to address the question of whether insulin aggregation occurs only

through a monomeric intermediate or may involve dimers and higher oligomers. The concept of a monomeric aggregation-competent intermediate is widespread; however, several findings and our own results cast doubts over it. First, it was noted that on the contrary to the "monomer" model, insulin aggregation is faster under conditions favoring dimers (e.g., HCl) than monomers (acetic acid) (*19*). Second, such a model is not supported by the concentration dependence of the DSC scans shown in Figure 6. While the decreasing temperature of the actual aggregation (exothermic peak) with increasing concentration is what one would expect for a "nucleation and growth" type of kinetics, the simultaneous shifting of the endothermic peak toward lower temperatures is somehow puzzling. In a solution containing dimers and monomers, as is the case of insulin samples acidified with HCl, increasing concentration is expected to shift the equilibrium toward dimers and, according to the model, reduce the fraction of aggregation-prone molecules (monomers). Figure 6 shows convincingly that this does not hold true for insulin. Third, consideration of the strong preventive effect that pressure has on insulin aggregation makes one more argument against the "monomer intermediate" concept. Namely, pressure is known to dissociate noncovalent protein assembles, such as multi-subunit proteins, protein oligomers, antigen−antibody complexes, and virus capsids (*34*). One of reasons to this is the fact that more water molecules can fill in the protein's void volume when it becomes accessible to solvent upon subunit dissociation. This leads to a total volume contraction and is hence favored under high pressure (*34*, *39*). On the other hand, solvent-exposure of charged groups that have been involved in stabilization of protein assemblies (as salt-bridges) also contributes to the overall volume reduction through the so-called electrostriction, which consists of a tightly packed arrangement of the solvent dipolar molecules around charged solutes (*40*). Another, yet still debated (e.g. ref *40*), factor influencing the pressure effect on polypeptide assemblies stems from the hydration of hydrophobic residues under high pressure (e.g., hydration volumes of model hydrocarbons such as benzene or methane are negative (*34*)). Outlining of these factors shows why protein assemblies driven by hydrophobic or electrostatic interactions, and, in addition, containing void volume are disfavored under high pressure. It is therefore expected that 300 bar pressure has, if any, a dissociating effect and shifts the monomer−dimer equilibrium to the left. The influence of such low pressure is clearly limited to tertiary or quaternary interactions, as the secondary structure sensitive amide I′ band remains unaffected under 300 bar. On the other hand, the pronounced volume expansion occurring when the aggregation-prone intermediate is formed creates a volumetric barrier that cannot be crossed by the conformation, should an external hydrostatic pressure be applied. The molecular scenario emerging from these results depicts the insulin aggregation process as taking place through a MG-like dimer, which unfolds into the actual aggregation-prone less-structured intermediate. This is followed by aggregation as such. Should moderately high pressure be applied, it will play a temperature-adverse role by preventing the occurrence of a space-consuming random coil conformation. It cannot be ruled-out, however, that the intermediate is not perfectly orderless and some dimer-like, or higher oligomer-like interchain contacts are preserved. If existence of these contacts is necessary for the aggregation of insulin, the contacts' further loosening and dissociation under high pressure would explain the pressure-induced hindering of aggregation in an alternative way. A recent work produced also considerable evidence pointing to a dimeric aggregation intermediate of transthyretin, a protein which used to be thought of as having a monomeric intermediate on its aggregation pathway (*41*).

The Aggregation Stage. The virtual independence of the endothermic peak from scan rate is in a stark contrast to the exothermic peak (Figure 6). The same was observed for the aggregation of C9 protein (*13*). In general, this kind of behavior may be attributed to the unfolding transition occurring under nonequilibrium conditions, as was revealed in a recent DSC study of streptokinase denaturation (*42*). A nonequilibrium behavior is certainly expected for a protein forming an amyloid. The DSC data are likely to reflect the fast (at the permissive temperature) unfolding of the native protein and the markedly slower aggregation stage. Formation of the intermediate is in fact more reversible than what Figure 7 seems to suggest. The proximity of both peaks makes it impossible to complete the first transition without entering the second one. Once a "seed" of the β-amyloid is formed, the process of its elongation and spreading will continue and the enthalpic costs of aggregation-competent intermediate will be covered directly by heat released in aggregation. This has been supported by an additional DSC experiment with scans ending at a "aggregation-free" temperature at the endothermic peak's height. It showed almost quantitative reversibility of the process. Regardless of the sign of enthalpic effects of aggregation, proteins generally share similar values of heat capacity changes of unfolding, $\Delta C_p \approx 2$ kJ mol^{-1} K^{-1} (*13*, *42*). ΔC_p reflects the fact that unfolding not only increases solvent accessible surface area (ASA) of a protein, but it also significantly increases the population of nonpolar, and therefore kosmotropic (water structure-making) amino acid side chains that move out of hydrophobic cores and become exposed to the solvent. Therefore, the smaller values of ΔC_p, the less structured the protein is. The putative reversibility of insulin unfolding is a good starting point for calculating ΔC_p. This, however, turned out to be virtually impossible due to the persistent overlap between the endothermic and the exothermic DSC peaks. A negative ΔC_p value of -2 kJ mol^{-1} K^{-1} was estimated as a difference between the heat capacity of fresh protein at 10 °C and the completely aggregated one at 70 °C. This value must be interpreted cautiously as it is likely to encompass both the difference in amino acid hydration between the amyloid and native protein, as well as a macroscopic-level precipitation of the amyloid and global reduction in solvent−solute interface. That the ΔC_p value depends on the scan rate only supports this claim as the morphology of amyloid fibrils and their effective surface strongly depends on the conditions and regimes under which they were obtained. The same explanation is plausible for the differences in relative volume changes estimated by PPC scans at different scan rates (Figure 8). When the effective scan rate value approaches 5 °C/h, the relative volume change increases up to 0.26% ($\pm$0.02). The negative slope of the α-vs-T plots is typical for proteins and reflects the predominantly chaotropic character of the solvent-exposed amino acid residues. When unfolding starts, a significant number of nonpolar and thus kosmotropic residues are freed from the

protein's interior, or, more precisely, from the protein hydrophobic core, and become exposed to water. Their water-structuring properties contribute not only to the overall volume effect, but they also affect the slope of the baseline under the peak. For a number of proteins studied, the PPC plots in the pre- and post-transition regions were negative, but had a positive baseline at the transition (*15*). This is more enigmatic in the case of insulin. According to the PPC plots, the slope levels off for the first time at 40 °C, before H/D-exchange is complete and while the protein retains its native secondary fold. This may correspond to a swelling MG state of insulin. The following decrease of α beyond 60 °C, namely, when the plot shows again a negative slope, can be envisaged as a rearrangement of hydrophobic residues allowing to reduce their exposure to the bulk solvent. Such an event is rational for the hydrophobically driven aggregation phase, which is initiated at this temperature.

Influence of the H_2O/D_2O Substitution. Since the infrared study was carried out in D_2O-based samples while most of the DSC, ITC, and PPC measurements used H_2O, it was useful to investigate how the isotopic substitution affects the calorimetric plots. The similar position of the endothermic DSC peak in both solvents justifies juxtaposition and comparative analyses of the temperature-dependent infrared spectra (Figures 1A and 2A) with the DSC and PPC scans. As the H_2O/D_2O substitution shifts only the exothermic peak, heavy water exhibits a stabilizing effect on the intermediate state rather than on the native structure. The ability of D_2O to stabilize proteins against aggregation has been implicated before (e.g., ref *43*), though without pinning it down to any particular phase of this process. It has been shown, however, that if instead of T_m actual ΔG values are taken as a gauge of protein stability, the D_2O stabilizing effect on proteins becomes more ambiguous due to enthalpy−entropy compensation (*44*). The latter phenomenon has again been attributed to changes in hydration of proteins in H_2O and D_2O. In a comparative DSC/PPC study on transitions in poly(*N*-isopropylacrylamide) in H_2O and D_2O, the coiled form of the polymer was said to be more extended, i.e., have larger polymer−solvent surface, in heavy water than in light water (*17*). This results in a larger amount of structured water in the former case. The larger amount of structured water explains well the larger absolute values of ΔC_p in heavy water because more heat is needed for melting of the structured solvent. Obviously, as the structured water is more space-consuming, this simultaneously explains the larger volume expansions in D_2O seen in PPC. Although, the H_2O/D_2O substitution seems to be the slightest perturbation one can induce in protein-solvating water system, the consequences of that change can be more intricate. Apart from the more pronounced protein-solvation and solvent-structuring effects, the influence of deuteration on the strength of hydrogen bonding should be taken into account. That the later one will vary with respect to the type of secondary structure involved, only further complicates determination of the mechanism of the substitution.

CONCLUSIONS

In conclusion, the coupling of infrared spectroscopy and ultra-sensitive scanning calorimetric techniques yields a very insightful approach to studying protein aggregation. That is so because the protein aggregation phenomenon, lying on the borderline between proteins as functional biological entities and proteins as polymers, is determined by the relation between their structure and hydration. We have shown that insulin aggregation occurs in two following phases, one of which includes loosening of the tertiary contacts and endothermic unfolding into a bulky intermediate, followed by slow, irreversible, and exothermic aggregation. According to the data, a possible mechanism of the aggregation-preventing influence of high pressure has been put forward.

REFERENCES

1. Sipe, J. D., and Cohen, A. S. (2000) *J. Struct. Biol. 130*, 88−98.
2. Jackson, G. S., and Clarke, A. R. (2000) *Curr. Opin. Struct. Biol. 10*, 69−74.
3. Serpell, L. C. (2000) *Biochim. Biophys. Acta 1502*, 16−30.
4. Goers, J., Permyakov, S. E., Permyakov, E. A., Uversky, V. N., and Fink, A. L. (2002) *Biochemistry 41*, 12546−12551.
5. Fandrich, M., Fletcher, M. A., and Dobson, C. M. (2001) *Nature 6825*, 165−166.
6. Fandrich, M., and Dobson, C. M. (2002) *EMBO J. 21*, 5682−5690.
7. Bouchard, M., Zurdo J., Nettleton, E. J., Dobson, C. M., and Robinson, C. V. (2000) *Protein Sci. 9*, 1960−1967.
8. Booth, D. R., Sunde, M., Bellotti, V., Robinson, C. V., Hutchinson, W. L., Fraser, P. E., Hawkins, P. N., Dobson, C. M., Radford, S. E., Blake, C. C. F., and Pepys, M. B. (1997) *Nature 385*, 787−793.
9. Ferrao-Gonzales, A. D., Souto, S. O., Silva, J. L., and Foguel, D. (2000) *Proc. Natl. Acad. Sci. U.S.A. 97*, 6445−6450.
10. Chiti, F., Webster P., Taddei, N., Clark, A., Stefani, M., Ramponi, G., and Dobson, C. M. (1999) *Proc. Natl. Acad. Sci. U.S.A. 96*, 3590−3594.
11. Fink, A. L. (1998) *Fold. Des. 3*, R9−R23.
12. Dzwolak, W., Kato, M., Shimizu, A., and Taniguchi, Y. (1999) *Biochim. Biophys. Acta 1433*, 45−55.
13. Lohner, K., and Esser, A. F. (1991) *Biochemistry 30*, 6620−6625.
14. Cooper, A., Johnson, C. M., Lakey, J. H., and Nollmann, M. (2001) *Biophys. Chem. 93*, 215−230.
15. Lin, L. N., Brandts, J. F., Brandts, J. M., and Plotnikov, V. (2002) *Anal. Biochem. 302*, 144−160.
16. Heerklotz, H., and Seelig, J. (2002) *Biophys. J. 82*, 1445−1452.
17. Kujawa, P., and Winnik, F. M. (2001) *Macromolecules 34*, 4130−4135.
18. Ravindra, R., and Winter, R. (2003) *ChemPhysChem 4*, 359−365.
19. Whittingham, J. L., Scott, D. J., Chance, K., Wilson, A., Finch, J., Brange, J., and Dodson, G. G. (2002) *J. Mol. Biol. 318*, 479−490.
20. Hua, Q. X., and Weiss, M. A. (1991) *Biochemistry 30*, 5505−5515.
21. Millican, R. L., and Brems, D. N. (1994) *Biochemistry 33*, 1116−1124.
22. Turnell, W. G., and Finch, J. T. (1992) *J. Mol. Biol. 227*, 1205−1223.
23. Nielsen, L., Frokjaer, S., Brange, J., Uversky, V. N., and Fink, A. L. (2001) *Biochemistry 40*, 8397−8409.
24. Jimenez, J. L., Nettleton, E. J., Bouchard, M., Robinson, C. V., Dobson, C. M., and Saibil, H. R. (2002) *Proc. Natl. Acad. Sci. U.S.A. 99*, 9196−9201.
25. Nielsen, L., Frokjaer, S., Carpenter, J. F., and Brange, J. (2001) *J. Pharm. Sci. 90*, 29−37.
26. Waugh, D. F. (1948) *J. Am. Chem. Soc. 70*, 1850−1857.
27. Sluzky, V., Tamada, J. A., Klibanov, A. M., and Langer, R. (1991) *Proc. Natl. Acad. Sci. U.S.A. 88*, 9377−9381.
28. Nielsen, L., Khurana, R., Coats, A., Frokjaer, S., Brange, J., Vyas, S., Uversky, V. N., and Fink, A. L. (2001) *Biochemistry 40*, 6036−6046.
29. Kwon, Y. M., Baudys, M., Knutson, K., and Kim, S. W. (2001) *Pharm. Res. 18*, 1754−1759.
30. Dzwolak, W., Kato, M., Porowski, S., and Taniguchi, Y. (2003) Insulin and polylysine as model polypeptides for FTIR studies of the pressure-effect on protein aggregation, in *Advances in High-Pressure Bioscience and Biotechnology II* (Winter, R., Ed.) pp 79−82, Springer-Verlag, Heidelberg.

31. Panick, G., and Winter, R. (2000) *Biochemistry 39*, 1862−1869.
32. Herberhold, H., and Winter, R (2002) *Biochemistry 41*, 2396−2401.
33. Barth, A. (2000) *Prog. Biophys. Mol. Biol. 74*, 141−173.
34. Gross, M., and Jaenicke, R. (1994) *Eur. J. Biochem. 221*, 617−630.
35. Boelens, R., Ganadu, M. L., Verheyden, P., and Kaptein, R. (1990) *Eur. J. Biochem. 191*, 147−153.
36. Goormaghtigh, E., Cabiaux, V., and Ruysschaert, J. M. (1994) *Subcell. Biochem. 23*, 405−450.
37. Chiou, J. S., Tatara, T., Sawamura, S., Kaminoh, Y., Kamaya, H., Shibata, A., and Ueda, I. (1992) *Biochim. Biophys. Acta 1119*, 211−217.
38. Rochu, D., Beaufet, N., Renault, F., Viguie, N., and Masson, P. (2002) *Biochim. Biophys. Acta 1594*, 207−218.
39. Mozhaev, V. V., Heremans, K., Frank, J., Masson, P., and Balny, C. (1996) *Proteins 24*, 81−91.
40. Boonyaratanakornkit, B. B., Park, C. B., Clark, D. S. (2002) *Biochim. Biophys. Acta 1595*, 235−249.
41. Serag, A. A., Altenbach, C., Gingery, M., Hubbell, W. L., and Yeates, T. O. (2001) *Biochemistry 40*, 9089−9096.
42. Azuaga, A. I., Dobson, C. M., Mateo, P. L., and Conejero-Lara, F. (2002) *Eur. J. Biochem. 269*, 4121−4133.
43. Verheul, M., Roefs, S. P. F. M., and de Kruif, K. G. (1998) *FEBS Lett. 421*, 273−276.
44. Makhatadze, G. I., Clore, G. M., and Gronenborn, A. M. (1995) *Nat. Struct. Biol. 2*, 852−855.

BI034879H